Measurement of the ^{2}H(d,^{2}He)^2n reaction at $E_d = 171$ MeV and implications for the neutron-neutron scattering length

C. Bäumer, D. Frekers, E.-W. Grewe, P. Haefner, S. Hollstein, B. C. Junk, A. Korff, S. Rakers, and R. Schmidt
Institut für Kernphysik, Westfälische Wilhelms-Universität Münster, D-48149 Münster, Germany

A. M. van den Berg, B. Davids,* M. N. Harakeh, M. Hunyadi,† M. A. de Huu,‡ and H. J. Wörtche
Kernfysisch Versneller Instituut, Rijksuniversiteit Groningen, NL-9747 AA Groningen, The Netherlands

N. Blasi
Istituto Nazionale di Fisica Nucleare, I-20133 Milano, Italy

D. De Frenne, E. Jacobs, A. Negret,§ and L. Popescu§
Vakgroep Subatomaire en Stralingsfysica, Universiteit Gent, B-9000 Gent, Belgium

R. De Leo
Istituto Nazionale di Fisica Nucleare, I-70126 Bari, Italy

F. Hofmann, P. von Neumann-Cosel, and A. Richter
Institut für Kernphysik, Technische Universität Darmstadt, D-64289 Darmstadt, Germany

(Received 22 November 2004; published 29 April 2005)

A measurement of the ^{2}H(d,^{2}He)^2n charge-exchange reaction at $E_d = 171$ MeV has been performed in order to study the interaction of the di-neutron system. Spectroscopy of the neutron-neutron final-state interaction with a resolution of about 115 keV (FWHM) was achieved by measuring the momentum of ^{2}He at forward scattering angles. In the experiment the two protons of the unbound ^{2}He are momentum analyzed with a magnetic spectrometer and detected with the same detector. A simple reaction theory is employed in order to obtain information about the neutron-neutron interaction from the measured cross section data. The validity of the impulse approximation for the $d \rightarrow {}^2$He transition at intermediate energies is discussed and compared to the Watson-Migdal theory of the proton-proton final-state interaction. Predictions of the impulse approximation for the analog transition $d \rightarrow {}^2n$ are confronted with experimental data. A procedure to extract the neutron-neutron scattering length a_{nn} from this comparison is presented. The result is compatible with the recommended value of $a_{nn} = -18.6(\pm 0.4)$ fm.

DOI: 10.1103/PhysRevC.71.044003 PACS number(s): 13.75.Cs, 24.10.Cn, 24.80.+y

I. INTRODUCTION

The $(d, {}^2\mathrm{He})$ reaction at intermediate energies ($E_d \gtrsim 100$ MeV) has been recognized as a viable and powerful probe to study nuclear structure and few-body dynamics [1]. By definition, ^{2}He is the singlet S state ($^1S_0$) of the unbound di-proton system. The term (d,^{2}He), thus, refers to a kinematical regime, where the two correlated protons have a low relative energy ε_{pp} ($\varepsilon_{pp} \lesssim 1$ MeV). Since projectile d ($J^\pi = 1^+, T = 0$) and ejectile ^{2}He ($J^\pi = 0^+, T = 1$) are connected by a Gamow-Teller (GT) transition, (d,^{2}He) induces exclusively isovector spin-flip excitations, and at forward scattering angles the transition connecting target and residual nucleus is highly selective owing to the dominance of the $V_{\sigma\tau}$ NN interaction, as shown e.g., in Ref. [2]. Assuming a one-step reaction mechanism, this allows a straight-forward interpretation in terms of the impulse approximation (IA). Unpolarized (d,^{2}He) reaction experiments were carried out investigating primarily GT and spin-dipole response in nuclei, as, e.g., described in Refs. [3,4]. Experiments with a polarized deuteron beam were performed for the same purpose (see, e.g., Ref. [5]) together with studies of the quasi-free region [6] and the Δ-resonance [7]. Note that the pioneering works employing polarized deuterons were spawned by a potential use of the (d,^{2}He) reaction in a deuteron polarimeter [8].

A particular interesting situation arises if deuterium is used as a target. In analogy to the projectile-ejectile transition $d \rightarrow {}^2$He, the GT transition operator equally prepares the di-neutron system in a $^1S_0$ state. The transition strength of $d \rightarrow {}^2n$ ($^1S_0$) as function of the internal neutron-neutron energy ε_{nn} can then be mapped out with high precision using (d,^{2}He) as a spectroscopic tool. Therefore, the ^{2}H(d,^{2}He)^2n reaction is one of the rare possibilities to study the elusive di-neutron system. As will be shown below, ^{2}H(d,^{2}He)^2n represents a means to infer the neutron-neutron scattering length a_{nn}, although the neutron-neutron system is observed in incomplete kinematics.

*Present address: TRIUMF, Vancouver, B. C., Canada.
†Present address: ATOMKI, Debrecen, Hungary.
‡Present address: Contrinex SA, Givisiez, Switzerland.
§Permanent address: NIPNE, Bucharest, Romania.

There have been similar endeavors to obtain a_{nn} through the ^{2}H$(n,p)\,^2n$ reaction [9–12], but the interpretation of the spectra was limited by the poor energy resolution of about 1 MeV. Note that the isobaric analogue transitions to the $^1S_0$ configuration of pp and np have been investigated in a similar way. For instance, Burzynski *et al.* measured ^{2}H$(p,p')d^*$ at forward angles and extracted $a_{np} = (-24.7 \pm 0.4)$ fm [13].

Since it is at present not possible to conduct any direct measurements of a_{nn} using free neutron-neutron collisions, all current values of a_{nn} are extracted from multiparticle reactions. Indirect information about a_{nn} has been gained from the following processes:

$$\pi^- + d \rightarrow \gamma + n + n, \tag{1}$$

$$n + d \rightarrow p + n + n. \tag{2}$$

Three independent studies with the electromagnetic probe [reaction (1)] have been performed at the Paul Scherrer Institut [14,15] and at the Los Alamos Meson Physics Facility (LAMPF) [16]. In Ref. [14] only the γ spectrum was measured, while the later experiments detected the γ and one neutron [15,16]. Reaction (1) has the advantage that it involves only two strongly interacting particles in the exit channel. The extracted values for a_{nn} agreed well, giving an average value of (-18.59 ± 0.40) fm [17]. A study at Triangle Universities Nuclear Laboratory with the hadronic reaction [Eq. (2)] yielded $a_{nn} = (-18.7 \pm 0.6)$ fm [18]. This value and that from the pion-capture experiment at LAMPF [16] constitute the "recommended" a_{nn} value (-18.6 ± 0.4) fm [17]. This value has to be further corrected for the magnetic interaction in order to get the "pure" nuclear value a_{nn}^N. Referring to Miller *et al.* [19] this correction varies between -0.35 and -0.33 fm. Note that the experiments of reaction type (2) are difficult to perform and require elaborate models to compare with. The experimental procedures and details of the analyses have recently gained renewed importance, since the Bonn neutron group has published its results of a new study of a_{nn} with neutron induced d breakup [Eq. (2)]. The extracted value is $a_{nn} = (-16.27 \pm 0.4)$ fm and $a_{nn} = (-16.06 \pm 0.35)$ fm, if the data are normalized to quasi-free scattering [20,21]. These values clearly disagree with the values cited above and imply a different interpretation of charge symmetry breaking (CSB). Note that the results agree with the recommended nn effective-range parameter of before 1978 [22].

A rather clean way to measure a_{nn} would be [22,23]

$$\mu^- + d \rightarrow n + n + \nu_\mu, \tag{3}$$

as the final state is not distorted by strong or electromagnetic interactions with a third particle. Considering today's experimental techniques and those of the near future, a measurement of reaction (3) is impossible. Reference [23] gives a detailed account of the experimental and theoretical features of muon capture on light nuclei.

Since the above-mentioned experiments show conflicting results for a_{nn}, there is need for a new type of experiment. It is argued in this work that the following reaction offers a novel way to obtain a_{nn}:

$$d + d \rightarrow {}^2\mathrm{He} + n + n, \tag{4}$$

where ^{2}He is measured at forward scattering angles and at an incident intermediate energy, where the GT transition is strong.

This article is structured as follows. We start with a general discussion of the $(d,{}^2\mathrm{He})$ reaction mechanism (Sec. II), keeping in mind that $d \rightarrow {}^2$He has to be treated analogously to the mirror transition $d \rightarrow {}^2n$. Experimental details are given in Sec. III and the data analysis is described in Sec. IV. In Sec. V the data are treated in leading order IA to obtain a_{nn}.

II. FEATURES OF THE $(d,{}^2\mathrm{He})$ REACTION

A. Charge-exchange reactions

Scattering at intermediate energies with nuclear probes or light ions is regarded to proceed as a direct, one-step reaction. In the impulse approximation it is assumed that effects of the nuclear medium in the target can be neglected at large incident energies compared to the Fermi energy of the nucleons in the target. The interaction between projectile and target nucleons is then modelled by an effective interaction, which is taken to be the free NN t_F matrix. A t_F matrix interaction, which is often used for the description of nuclear reactions, is the effective interaction of Franey and Love [24,25]. With these assumptions, the transition amplitude has the form [26]

$$\mathcal{T}_{fi}^{DW}(\vec{k_f},\vec{k_i}) = \int d^3q\, D(\vec{k}_f,\vec{k}_i,\vec{q}\,)\, U_{fi}^{\alpha}(\vec{q}\,)\rho_p^{\beta}, \qquad \alpha = \tau,\ \sigma\tau,\ T\ ;\ \beta = \tau,\ \sigma\tau, \tag{5}$$

where $\vec{q} = \vec{k}_f - \vec{k}_i$, and the interaction-weighted nuclear responses (nuclear transition potentials) are given by [26]

$$U_{fi}^{\tau}(\vec{q}\,) = t_\tau^C(\vec{q}\,)\rho_{fi}^{\tau}(\vec{q}\,), \quad \Delta S = 0, \tag{6}$$

$$U_{fi}^{\sigma\tau}(\vec{q}\,) = t_{\sigma\tau}^C(\vec{q}\,)\rho_{fi}^{\sigma\tau}(\vec{q}\,), \ \Delta S = 1, \tag{7}$$

$$U_{fi}^{T}(\vec{q}\,) = t_{\sigma\tau}^T(\vec{q}\,)\rho_{fi}^{\sigma\tau}(\vec{q}\,), \quad \Delta S = 1. \tag{8}$$

The nuclear transition potentials are defined for non-spin-flip transitions ($\Delta S = 0$) and spin-flip transitions ($\Delta S = 1$), where the latter consists of a central part (C) and a tensor part (T). The terms t_τ^C, $t_{\sigma\tau}^C$, and $t_{\sigma\tau}^T$ refer to the isovector non-spin-flip part, isovector spin-flip part, and tensor part, respectively, of the effective interaction [24,25]. Target transition densities are defined according to the relation [26]

$$\rho_{fi}^{\sigma\tau}(\vec{q}\,) = \langle\Psi_f|\sum_{j=1}^{A} e^{i\,\vec{q}\cdot\vec{r}_j}\vec{\sigma}(j)\vec{\tau}(j)|\Psi_i\rangle, \tag{9}$$

where $|\Psi_{i/f}\rangle$ are the initial (i) and final (f) state, respectively. The sum in the above equations runs over all nucleons of the target. For non-spin-flip transitions (ρ_{fi}^{τ}) the spin operator $\vec{\sigma}(j)$ is replaced by the identity operator. The projectile transition density is given accordingly [26,27]:

$$\rho_p^{\beta} = \langle p'|\textstyle\sum_k e^{i\,\vec{q}\cdot\vec{r}_k}\,\Gamma_k|p\rangle,\ \Gamma_k = \vec{\tau}_k, \vec{\sigma}_k\vec{\tau}_k \ \text{ for } \beta = \tau,\ \sigma\tau, \tag{10}$$

where p denotes the projectile and p' the ejectile. $D(\vec{k}_f, \vec{k}_i, \vec{q}\,)$ is the projectile/ejectile distortion function defined by [26,27]

$$D(\vec{k}_f, \vec{k}_i, \vec{q}\,) = \frac{1}{(2\pi)^3} \int d^3r_p\, \chi_f^*(\vec{k}_f, \vec{r}_p)\, e^{-i\,\vec{q}\cdot\vec{r}_p}\, \chi_i(\vec{k}_i, \vec{r}_p). \tag{11}$$

The distorted waves $\chi_{f/i}$ describe the relative motion of projectile and target before and after the charge-exchange event. Note that $D(\vec{k}_f, \vec{k}_i, \vec{q}\,) = \delta(\vec{q} - \vec{k}_i + \vec{k}_f)$ in the plane-wave approximation (PWA).

B. Final-state interaction of the $(d,^2$He) reaction

The reaction mechanism of the $(d,^2$He) reaction is discussed in the framework of the impulse approximation. For a description in the distorted-wave Born approximation (DWBA) we refer to Ref. [28].

A feature of the $(d,^2$He) probe is that the interaction of the projectile can be assumed to take place between the target nucleons and one constituent of the projectile (the neutron), while the other part (the proton) continues undisturbed. Since projectile and ejectile are connected by a Gamow-Teller transition, only the transition densities $\rho_{fi}^{\sigma\tau}(\vec{q}\,)$ and $\rho_p^{\sigma\tau}(\vec{q}\,)$ contribute to the transition amplitude of Eq. (5). Thus, in the case of the $(d,^2$He) reaction the (complex) structure of projectile and ejectile enhances the selectivity of the probe compared to the simple spectator-model, i.e., the (n,p) reaction. It is helpful to note that the projectile $\rightarrow$ ejectile transition resembles the inverse process of the weak proton capture, which mediates hydrogen burning in the sun:

$$p + p \;\rightarrow\; {}^2\mathrm{He} \rightarrow d + e^+ + \nu_e. \tag{12}$$

Obviously the $(d,^2$He) reaction is complicated by having three particles in the final state. It is generally assumed that the ejectile is first produced in a particle unstable state, which will subsequently decay. The sequential process proceeds through the formation of the intermediate state ^{2}He and the subsequent decay into two protons [29]:

$$d + A \rightarrow {}^2\mathrm{He} + B \rightarrow p + p + B. \tag{13}$$

The relative energy between the two protons is given by the expression

$$\varepsilon_{pp} = \tfrac{1}{2}\mu_{1-2} v_{1-2}^2 = [E_1 + E_2 - 2\sqrt{E_1\,E_2}\cos\Theta_{1-2}], \tag{14}$$

where E_1 and E_2 are the laboratory energies of the two protons, $\Theta_{1-2} = \Theta_{pp}$ is their relative angle, and μ_{1-2} is the reduced mass of the di-proton system [1]. Concerning Eq. (13), we consider only experiments which are kinematically complete, i.e., the horizontal and vertical angles of both protons are detected along with their energies E_1 and E_2. That allows, in addition to ε_{pp}, the determination of the scattering angle $\Theta_{^2\mathrm{He}}$ and the total kinetic energy (TKE) $E_{^2\mathrm{He}} = E_1 + E_2$. Note that $E_d = E_{^2\mathrm{He}} + E_x + E_{\mathrm{recoil}} + Q$, where E_d is the energy of the incoming deuteron and E_x is the excitation energy in the residual nucleus ($E_x = \varepsilon_{nn}$ in this work). A projection of the data on TKE means that all events are normalized to $\varepsilon_{pp} = 0$. Because the limited angular and momentum acceptance of the spectrometer in the experiment has a bearing on the shape of the so-obtained excitation energy spectra, a theoretical treatment of the sequential breakup is essential. To a large extent, this is governed by phase-space considerations. The phase-space factor for breakup of ^{2}He in the $B+^2$He system can be written as [29]

$$\rho(\varepsilon_{pp}) = p_{B-12}\,\mu_{B-12}\,p_{1-2}\,\mu_{1-2}\,d\Omega_{B-12}\,d\Omega_{1-2}/(2\pi\hbar)^3, \tag{15}$$

where momenta are denoted by p and reduced masses designated by μ. The relative motion of the two protons in the di-proton system is indicated by the index $1-2$, and the index $B-12$ refers to the motion of residual nucleus B relative to the center of mass of the two protons. The triple differential cross section for a sequential process now reads ($\varepsilon = \varepsilon_{pp}$) [29]

$$\frac{d^3\sigma}{d\Omega_{B-12}\,d\Omega_{1-2}\,d\varepsilon} = \frac{\mu_i\mu_{B-12}}{(2\pi\hbar^2)^2}\,\frac{k_{B-12}}{k_i}\,|\mathcal{T}_{fi}|^2\,\frac{\mu_{1-2}\,p_{1-2}}{(2\pi\hbar)^3}. \tag{16}$$

The projectile transition density defined in Eq. (10) can be written as

$$\rho_p^{\sigma\tau}(\vec{q}\,) = \langle\Psi_{^2\mathrm{He}}|\sum_{j=1}^{2} e^{i\,\vec{q}\cdot\vec{r}_j}\,\vec{\sigma}(j)\tau^+(j)|\Psi_d\rangle. \tag{17}$$

Deuteron charge-exchange reactions and the solar weak proton-capture defined in Eq. (12) can be described on the same footing through the matrix element in the above equation. Detailed information is furnished in Refs. [30,31]. The matrix element in Eq. (17) can be factorized into spin and spatial parts. After reduction, the spin part M_S is chosen such that $M(\mathrm{GT}) = 6$ [30]. The spatial component of the transition amplitude, which contains the dependence on ε_{pp}, is given by the overlap of the two-nucleon wave functions $|\Phi_{^2\mathrm{He}}\rangle$ and $|\phi_d\rangle$ [32]

$$\rho_p^{\sigma\tau}(\vec{q}, \varepsilon_{pp}) = M_S\langle\Phi_{^2\mathrm{He}}(\varepsilon_{pp})|\sum_j e^{i\,\vec{q}\cdot\vec{r}_j}|\Phi_d\rangle. \tag{18}$$

Because the above equation deals with nearly spherical wave functions, only the radial dependence has to be considered. The S-wave part of the deuteron wave function can be approximated by an analytic expression [33]

$$\Phi_d(r) = (e^{-0.232\,r} - e^{-1.202\,r})/r. \tag{19}$$

A better approximation is provided by calculations with modern nucleon-nucleon potentials. In this work the Argonne v18 potential is used [34]. As modern NN potentials exactly reproduce the deuteron density distribution, calculations with the Nijmegen potential, Reid soft core potential, etc., all lead to the same results. The scattering wave function $\Phi_{^2\mathrm{He}} = \Phi_{pp}$ depends on the separation r of the two nucleons and their relative momentum $k = p_{1-2}$,

$$\Phi_{NN} = e^{i\delta(k)}[F_0(k\,r)\cos\delta(k) + G_0(k\,r)\sin\delta(k)]/(k\,r), \quad \text{for } NN = pp, \tag{20}$$

$$\Phi_{NN} = e^{i\delta(k)}[\sin(k\,r)\cos\delta(k) + \cos(k\,r)\sin\delta(k)]/(k\,r), \quad \text{for } NN = nn, np. \tag{21}$$

F_0 and G_0 are the regular and irregular S-wave Coulomb wave functions. Equation (21) refers to the case of an uncharged

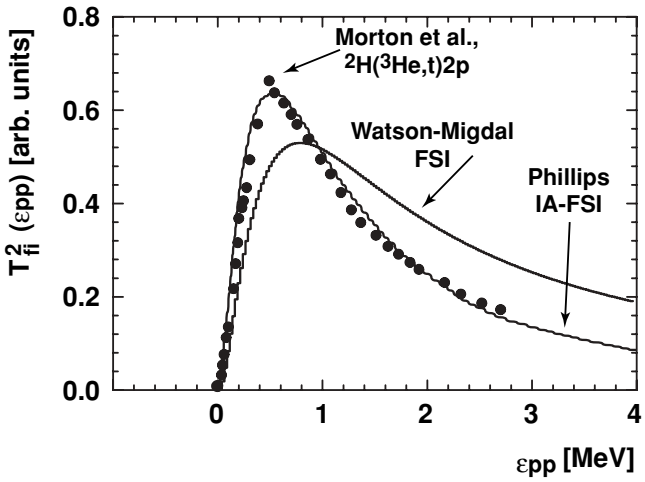

FIG. 1. Square of the calculated transition amplitudes including the appropriate phase-space factor for the $d \rightarrow {}^2\mathrm{He}$ transition. The solid curves indicate the FSI model of Watson and Migdal [36,37] and the impulse approximation model of Phillips [32], respectively. The latter distribution is also predicted by the DWBA code ACCBA at forward angles [28]. Filled circles represent the outcome of a ${}^2\mathrm{H}({}^3\mathrm{He}, t)2p$ reaction measurement at $\approx 0^\circ$ using a 74 MeV ${}^3\mathrm{He}$ beam [38]. The maximum energy ε_{pp} observed in this experiment is about 2.7 MeV. The respective distributions are not to scale in the vertical direction.

ejectile. It will be needed for the discussion of the ${}^2\mathrm{H}(d,{}^2\mathrm{He})^2n$ reaction and is listed here to illustrate the effect of the Coulomb force in the exit channel. In the limit of $k \rightarrow 0$, the NN phase-shift $\delta(k)$ is related to the scattering length a_{NN} and the effective range r_{NN} by [35]

$$C^2\, k \cot\delta(k) \,+\, h(\eta)/R \,=\, -1/a_{NN} + \tfrac{1}{2} r_{NN} k^2. \qquad (22)$$

To complete the definitions, $R = 28.8$ fm, $\eta = e^2/(\hbar v_{1-2})$, $C^2 = 2\pi\eta/(e^{2\pi\eta} - 1)$, and $h(\eta) = -\ln\eta + \mathrm{Re}\,\Gamma'(1 + i\eta)/\Gamma(1 + i\eta)$ [35]. For $NN = np$, nn the Coulomb penetration factor $C^2(\eta) = 1$ and $h(\eta) = 0$.

The integral in Eq. (18), which reflects the overlap of Φ_{NN} and Φ_d, has to be calculated numerically. Figure 1 depicts the theoretical prediction for the pp final-state interaction (FSI) defined in Eqs. (15) and (17) as calculated by Phillips [32], who was the first to develop a model of deuteron charge-exchange reactions at forward angles. At $\varepsilon_{pp} \rightarrow 0$ the FSI is determined by the decreasing phase space $[\rho(\varepsilon_{pp}) \propto \sqrt{\varepsilon_{pp}}]$. Since the overlap $|\langle\Phi_{pp}|\Phi_d\rangle|^2$ has a maximum at $\varepsilon_{pp} \approx 300$ keV, the term $\rho(\varepsilon_{pp})\,|\langle\Phi_{pp}|\Phi_d\rangle|^2$ has a maximum at about 0.5 MeV. Several experiments have been performed to study the pp FSI with charge-exchange reactions.

Cross section and polarization transfer measurements of the ${}^2\mathrm{H}(p, n)2p$ reaction at forward angles have been performed at IUCF [39] ($E_p = 160$ MeV) and RCNP [40] ($E_p = 346$ MeV). However, these measurements suffer from a poor energy resolution. A ${}^2\mathrm{H}({}^3\mathrm{He}, t)2p$ experiment at $\Theta_{\mathrm{lab}} \approx 0^\circ$ and $E_{{}^3\mathrm{He}} = 74$ MeV is reported in Ref. [38]. Figure 1 also shows the excitation energy spectrum from this experiment. The shape of the measured distribution is in good agreement with the IA prediction.

A competing final-state interaction model, successfully applied in meson production reactions [41], has been introduced by Migdal and Watson [36,37]. This approach assumes that the final-state two-particle interaction alone is responsible for the internal energy distribution of the ejectile intermediate state. The following expression describes the corresponding transition amplitude for an $X \rightarrow pp$ S-wave FSI [35,42]:

$$\left|\mathcal{T}_{fi}^{pp}\right|^2 = \frac{C^2(\eta)}{C^4(\eta)\varepsilon_{pp} + (\hbar^2/m_p)\left[-a_{pp}^{-1} - h(\eta)/R + \gamma_p\varepsilon_{pp}\right]^2}, \qquad (23)$$

where $\gamma_p = r_e m_p/(2\hbar^2)$. The resulting distribution for $\rho(\varepsilon_{pp})|\mathcal{T}_{fi}|^2$ is displayed in Fig. 1, too. Compared to the IA calculation the FSI enhancement of the Watson-Migdal approach is broader and the fall-off shallower at higher ε_{pp}. Note that without FSI the corresponding distribution would have a $\sqrt{\varepsilon_{pp}}$ dependency. Migdal defines three conditions as prerequisite for the use of his model. Two of them are fulfilled in $(d,{}^2\mathrm{He})$ reactions: the primary cross section is determined by a short-range interaction and the unbound two-particle system is considered at low relative energies. However, the $(d,{}^2\mathrm{He})$ reaction obviously does not comply with the last condition, which states that the FSI must be strong and attractive. As the di-proton is generated from a deuteron configuration, where proton and neutron spend a considerable part of time outside the range of mutual interaction ($R_d \approx 4.3$ fm), contributions of the strong interaction (short range) are suppressed and the influence of the long-range Coulomb force is relatively strong. It is obvious from Fig. 1 that the Watson-Migdal FSI disagrees with the experimental finding of Ref. [38]. For reactions at high momentum transfer, however, the last condition is met in good approximation [41]. Okamura points out that in the case of $(d,{}^2\mathrm{He})$ the IA approach of Phillips gives a good description of the FSI for scattering angles $\Theta_{{}^2\mathrm{He}} \approx 0^\circ$ and the Watson-Migdal theory an adequate description for $\Theta_{{}^2\mathrm{He}} > 15^\circ$ [28]. A coherent treatment of the $(d,{}^2\mathrm{He})$ reaction at forward scattering angles is therefore given by an IA ($q \approx 0$) calculation of all partial transition densities.

A convention for $(d,{}^2\mathrm{He})$ reaction cross sections, often used in experiments probing the spin-isospin response of nuclei, is that ${}^2\mathrm{He}$ is equivalent to the pp FSI interaction up to $\varepsilon = \varepsilon_{pp} = 1$ MeV,

$$\frac{d\sigma}{d\Omega}[(d,{}^2\mathrm{He})] = \int_{\varepsilon_{\min}}^{\varepsilon_{\max}} d\varepsilon \int_{4\pi} d\Omega_{1-2} \frac{d^3\sigma}{d\Omega\, d\varepsilon\, d\Omega_{1-2}}, \qquad (24)$$

with $\varepsilon_{\min} = 0$ and $\varepsilon_{\max} = 1$ MeV.

Note that in some publications the right-hand side of the above equation contains an additional factor 1/2 accounting for the indistinguishability of two protons. This factor is not necessary when the ${}^2\mathrm{He}$ wave function $|\Psi_{{}^2\mathrm{He}}\rangle$ is by construction antisymmetric or both protons are detected in an experiment. Confining ε_{pp} to 1 MeV ensures that the di-proton system has indeed a ${}^1S_0$ configuration. This has been confirmed in an experiment where analyzing powers for ${}^1\mathrm{H}(d, 2p)n$ ($E_d = 200$ MeV) were determined [8]. A P state has zero amplitude at $\varepsilon_{pp} = 0$ MeV and only rises slowly to values of a few percent at about 1 MeV [7]. The integration in Eq. (24) bears on the term $p_{1-2} \cdot \rho_p^{\sigma\tau}(\vec{q}, \varepsilon_{pp})$ of

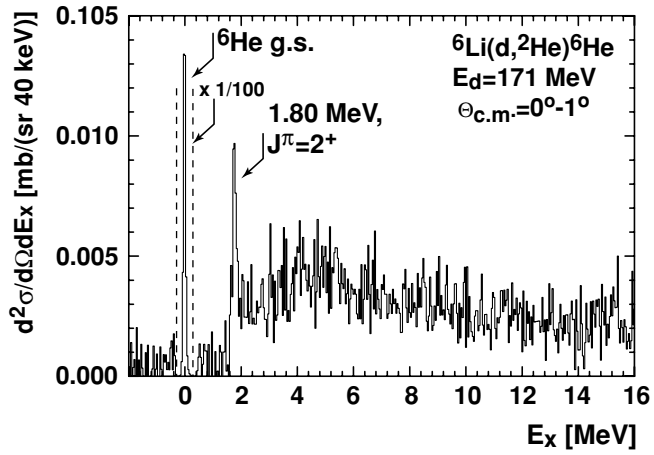

FIG. 2. Excitation energy spectrum of the ^{6}Li(d,^{2}He)^{6}He reaction at forward scattering angles. The cross section within the interval -0.35 MeV $\leqslant E_x \leqslant 0.35$ MeV, indicated by the dashed lines, has been downscaled by a factor 100. See Ref. [47] for further details.

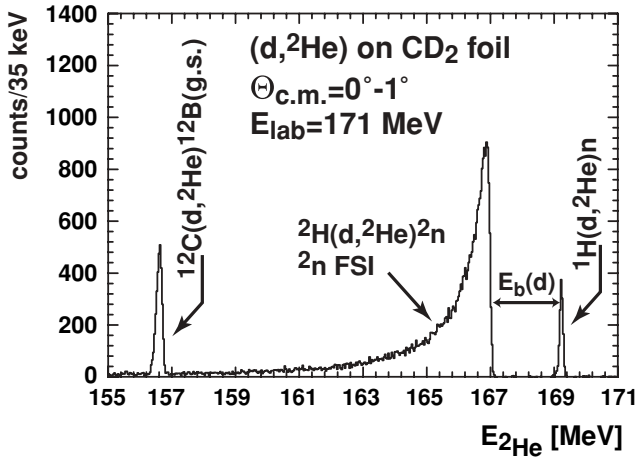

FIG. 3. Zero-degree spectrum of a (d,^{2}He) reaction measurement using a deuterated polyethylene foil (CD_2). The spectrum represents about half of the data which were taken at $\Theta_{BBS} = 0^\circ$. The spectrum has not been corrected for the limited detection probability for ^{2}He. The kinematics of ^{2}H(d,^{2}He)^2n was assumed for the recoil correction. The energy resolution is about 115 keV (FWHM).

Eqs. (16) and (17) reducing the projectile transition density for $d \rightarrow {}^2$He to a form which is equivalent to Eq. (10). Hence, the (d, ^{2}He) reaction can be regarded as (n,p)-type reaction with a quasi-bound ejectile.

An additional reaction channel in (d,^{2}He) might be given by deuteron breakup and a subsequent charge exchange from the incident continuum to the final scattering state [28,43]. In fact, cross sections for deuteron breakup at forward scattering angles can be several magnitudes larger than the respective (d,^{2}He) cross sections. Since the dependence of the breakup cross section on the atomic number Z is approximately quadratic, the reaction channel mentioned above can be neglected for ^{2}H(d,^{2}He). We refer to Ref. [43] for a DWBA description which incorporates coupling to the continuum. Further information about the (d,^{2}He) reaction mechanism with special emphasis to polarization observables is furnished in works of Bugg and Wilkin [44–46].

In order to substantiate the validity of the impulse approximation for $d \rightarrow {}^2$N ($N = n,p$), a similar transition is discussed: the ground state transition ^{6}Li $\rightarrow$ ^{6}He ($J_i^\pi = 1^+$, $J_f^\pi = 0^+$). In a simple model the target ^{6}Li can be regarded as cluster of an α-particle and a deuteron. Since the GT strength within the α-particle is Pauli blocked, GT transitions from ^{6}Li must proceed through its deuteron component giving $B(\mathrm{GT}) = 2$. Hence, the ^{6}Li(d, ^{2}He) reaction can be approximated as the ^{2}H(d,^{2}He) reaction with an α-particle as spectator. Actually the GT strength is quenched [$B(\mathrm{GT}^+) = 1.59$] and ^{6}He is a Borromean system, but this has little impact on the features of the reaction considered here. A measurement of the ^{6}Li(d,^{2}He) reaction has been carried out with a self-supporting lithium foil (99% enrichment ^{6}Li) at scattering angles close to 0° [47,48]. The outcome for $\Theta_{\mathrm{c.m.}} < 1^\circ$ is shown in Fig. 2. The excitation energy spectrum is dominated by the strong ground-state transition. Cross sections for excitations with $\Delta L > 0$ are about two orders of magnitude lower [47]. This clearly demonstrates that (d,^{2}He) at $q \approx 0$ fm^{-1} on light nuclei selectively excites Gamow-Teller states, if such transitions are favored by nuclear structure.

III. EXPERIMENT

The measurements were performed at the AGOR facility of KVI Groningen employing the magnetic Big-Bite Spectrometer (BBS) [49] in conjunction with the ESN-detector [50,51]. Unpolarized deuterons were accelerated by the superconducting cyclotron AGOR up to $E_d = 171$ MeV. Measurements have been performed at spectrometer angles $\Theta_{BBS} = 0^\circ, 3^\circ, 5^\circ, 8^\circ$. A deuterated polyethylene foil (CD_2) with an areal density of 7.2 mg/cm^2, which contained deuterium together with carbon and hydrogen, was used as target. Reference measurements with a self-supporting carbon target (natural enrichment) were carried out alternatingly in the same beam period. The primary beam was stopped in a Faraday cup located inside the BBS. Details of the experimental procedure are described in Ref. [52]. In order to provide the energies E_1 and E_2 and the vertical and horizontal angles, respectively, outgoing protons were momentum analyzed with the BBS and detected in coincidence at the focal-plane with the ESN-detector. The major building blocks of the ESN-detector are a focal-plane detection system (FPDS), which consists of two vertical drift chambers (VDCs), and a focal-plane polarimeter (FPP) consisting of four multiwire proportional chambers (MWPCs). In addition, two scintillator planes, which form the basis of the trigger system, are mounted at the entrance and exit of the FPP. The track reconstruction efficiency of the FPDS has been evaluated to be about 96%. This value stays constant over the entire focal plane, as has been shown in singles experiments with protons, deuterons, and α-particles, respectively. Since the entries at a certain energy $E_{^2\mathrm{He}}$ in the spectra (see, e.g., Figs. 2 and 3) are composed of proton pairs which intercept the focal plane within a considerable range, possible minor inhomogeneities of the efficiency average out.

IV. DATA ANALYSIS AND RESULTS

A. Energy spectra

The analysis of data from $(d,^2\mathrm{He})$ reaction experiments with the BBS+ESN setup is detailed in Ref. [52]. This section, therefore, deals only with some peculiarities of the data analysis regarding a CD_2 target. First, the accidental background, which stems from random coincidences of protons from the deuteron breakup, is considered. Since the target contains components with rather low Z, the accidental background is not a limiting factor. The prompt-to-random ratio is about $11:1$ for $\Theta_{\mathrm{c.m.}} < 1^\circ$. In accordance with Ref. [52] the contribution of accidental coincidences is subtracted from the raw spectra yielding excitation energy spectra which are free of experimental background. Second, the responses from ^{1}H, ^{2}H, and ^{12}C are widely separated by their respective Q-values. This is a distinctly advantageous situation, because the energy ($E_{^2\mathrm{He}}$ or ε_{nn}) can be calibrated in an independent way and with high precision. For the fundamental process $^1\mathrm{H}(d,^2\mathrm{He})n$ the deuteron is dissociated. Thus, the Q-value corresponds to the deuteron binding energy $E_b(d) = 2.224$ MeV. The reaction $^2\mathrm{H}(d,^2\mathrm{He})^2n$ has a Q-value of -4.449 MeV, because two deuterons are dissociated. For the ground state transition of $^{12}\mathrm{C}(d,^2\mathrm{He})^{12}\mathrm{B}$, which is discussed in Ref. [2], the Q-value is -14.811 MeV. There are no other contaminating reactions between the hydrogen peak and the carbon peak.

An example of a raw spectrum measured at $\Theta_{\mathrm{BBS}} = 0^\circ$ is shown in Fig. 3. The $^1\mathrm{H}(d,^2\mathrm{He})n$ reaction marks the high energy side of the spectrum. The response of $^2\mathrm{H}(d,^2\mathrm{He})^2n$ extends from its high-energy edge ($E_{^2\mathrm{He}} \approx 167.0$ MeV) to the ground state transition $^{12}C \rightarrow ^{12}\mathrm{B}$ ($E_{^2\mathrm{He}} \approx 156.6$ MeV). The scale of the energy axis, which was derived from calibration of the momentum deviation $\delta = \Delta p/p$ using single protons or light ions, is in agreement with the above mentioned calibration procedure using the ^{1}H, ^{2}H, and ^{12}C components. That one is, however, slightly more difficult to evaluate, because the projection on $E_{^2\mathrm{He}}$ depends on the recoil correction which in turn depends on the kinematics of the reaction. The estimate for the accuracy of $E_{^2\mathrm{He}}$ is 35 keV over the full excitation range of about 10 MeV, which was centered in the middle of the focal plane. An energy resolution ΔE of 115 keV (FWHM) was obtained, which was deduced from the neutron peak of the $^1\mathrm{H}(d,^2\mathrm{He})n$ reaction. Measurements at $\Theta_{\mathrm{BBS}} = 0^\circ$ were performed with dipole field settings $B = 0.5905$ T, $B = 0.5957$ T, and $B = 0.6115$ T. The resulting spectra agreed after acceptance corrections within the statistical errors.

B. Momentum dependence of $d\sigma/d\Omega$

Differential cross sections were obtained according to Eq. (24). Due to the limited momentum acceptance and limited solid angle of the BBS, not all correlated protons from ^{2}He are detected. A simulation software accounts for the reduced detection probability for ^{2}He by correcting the experimental energy spectra accordingly. The main ingredients of the simulation software are the matrices for beam transport within the BBS and a model for the proton-proton FSI. The former has been evaluated by means of sieve-slit measurements using various reactions [53,54]. The latter introduces a model dependence of differential cross sections of the $(d,^2\mathrm{He})$ reaction. This issue will be discussed in Sec. IV C.

The three cross section measurements at $\Theta_{\mathrm{BBS}} = 0^\circ$ were averaged with their respective statistical weights. Angle bins were defined for $0^\circ < \Theta_{\mathrm{c.m.}} \leqslant 1^\circ$ and $1^\circ < \Theta_{\mathrm{c.m.}} \leqslant 2^\circ$. As fewer statistics was available for the measurements at larger spectrometer angles, each of the $\Theta_{\mathrm{BBS}} = 3^\circ, 5^\circ, 8^\circ$ measurements was projected into one angle bin. Problems with the beam current integration occurred during the measurement at $\Theta_{\mathrm{BBS}} = 3^\circ$, so the cross section of this setting is normalized to the ground state transition $^{12}\mathrm{C} \rightarrow ^{12}\mathrm{B}$. The response of the $d \rightarrow {}^2n$ transition up to internal energies of about 3.1 MeV was subdivided in four bins of about equal integrated strength. Figure 4 shows the measured differential cross section as function of the scattering angle for the four energy bins. The angular distributions were calculated with the DWBA code ACCBA [28]. Note that the reaction $^2\mathrm{H}(d,^2\mathrm{He})^2n$ requires a fully microscopic calculation (see Sec. VI). An optical model, which describes entrance and exit channels, is not well defined for such a light system. However, as ACCBA is the only available reaction code for $(d,^2\mathrm{He})$, it was used for DWBA and plane-wave Born approximation (PWBA) calculations. The spectroscopic amplitude S_{ph} for the transition of a $0s_{1/2}$ proton to a $0s_{1/2}$ neutron was arbitrarily set to 1. A $J_i^\pi = 1^+$ to $J_f^\pi = 0^+$ transition was assumed. For the DWBA calculation the optical model parameters for the $(d,^2\mathrm{He})$ reaction on ^{12}C were taken [2,55]. Calculated cross sections were scaled to match the measured data (see Fig. 4). As can be seen from Fig. 4, there is little difference between DWBA and PWBA calculations. The falloff at larger scattering angles is slightly more pronounced than in the case of PWBA. By and large, both calculations agree with the data. For the first two energy bins ($\varepsilon_{nn} < 1.06$ MeV), the calculations slightly underestimate the falloff of $d\sigma/d\Omega$. This effect is reversed for the last energy bin (1.78 MeV $< \varepsilon_{nn} <$ 3.1 MeV). The four angular distributions considered here support the assumption, that $^2\mathrm{H}(d,^2\mathrm{He})^2n$ proceeds through a GT^+ transition.

The momentum transfer q of the response of $^2\mathrm{H}(d,^2\mathrm{He})^2n$ plotted in Fig. 3 ranges between 0.05 and 0.18 fm^{-1}. An extrapolation to $q = 0$ was performed according to the equation

$$\frac{d\sigma(q=0)}{d\Omega} = \frac{\sigma_{\mathrm{calc}}(q=0)}{\sigma_{\mathrm{calc}}(\Theta,q)} \frac{d\sigma_{\mathrm{exp}}(\Theta,q)}{d\Omega} \tag{25}$$

using the cross section data σ_{exp} at the most forward angles ($0^\circ - 1^\circ$). Because the cross-section ratio for finite q and $q = 0$ depends mainly on the kinematics and the momentum profile of $t^C_{\sigma\tau}$, PWBA calculations and DWBA calculations yield the same corrections for the transformation to $q = 0$. Figure 5 demonstrates the extrapolation for $\varepsilon_{nn} < 3.5$ MeV.

C. Proton-proton final-state interaction

The transition $d \rightarrow {}^2$He, which has already been discussed above, is now confronted with the data of the present experiment. The excitation of the pp system is measured

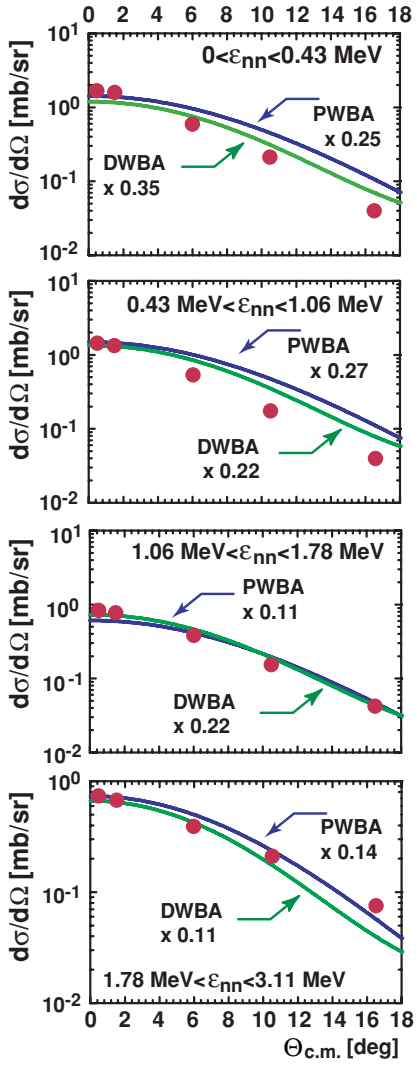

FIG. 4. (Color online) Angular distribution of $d\sigma/d\Omega$. The strength distribution for ^{2}H(d,^{2}He)^2n depicted in Figs. 3 and 5 has been divided into energy intervals of nearly equal integrated strength. Internal nn energies ε_{nn} up to about 3.1 MeV were taken into account. Semi-microscopic calculations with the code ACCBA are indicated with solid curves. Optical model parameters for ^{12}C(d,^{2}He) were taken for the DWBA calculation. Note that the DWBA code has no predictive power for the absolute strength within the intervals, and the corresponding scaling factors for DWBA and PWBA calculations are scaled to match the experimental cross sections.

according to Eq. (14) up to about 1 MeV with the (d,^{2}He) mode of the BBS+ESN setup. Figure 6 displays the experimental data for $d \rightarrow {}^2$He. Just as in Fig. 1, the predictions of the Watson-Migdal FSI and the IA-FSI are both plotted (Fig. 6 left). The distributions of the two final-state interaction models are also corrected for the acceptance of the BBS to allow a direct comparison with the experimental data. This can be more clearly seen in the right diagram of Fig. 6, where the experimental data are shown together with model distributions that incorporate the acceptance of the BBS and the limited energy resolution. Note that the reduced two-track efficiency for two-track distances $\Delta X \lesssim 5$ mm [52] has not

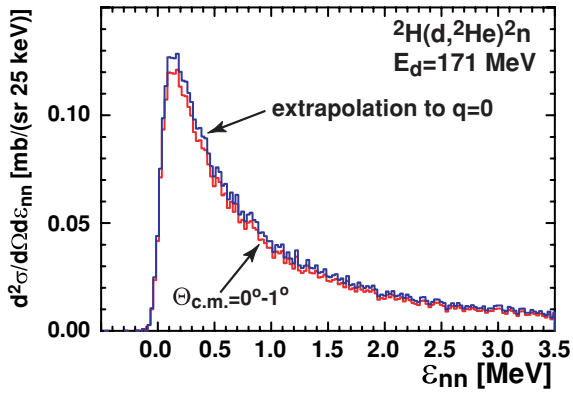

FIG. 5. (Color online) Extrapolation of the cross section measured at $0^\circ < \Theta_{\rm c.m.} \leqslant 1^\circ$ to $q = 0$. The ratio $\sigma(q = 0)/\sigma(q)$ has been determined by means of a DWBA calculation with the code ACCBA.

been incorporated. This only slightly affects the shape of the ε_{pp} distribution shown in Fig. 6. Due to the particular kinematics of the ^{2}H(d,^{2}He) reaction the di-proton acceptance of the BBS is even more limited ($\varepsilon_{pp} < 0.8$ MeV) than in other (d,^{2}He) studies performed so far ($A \geqslant 6$). The strength of the model distributions has been normalized to the integrated strength of the experimental data up to $\varepsilon_{\rm max} = 0.8$ MeV. In correspondence with the equivalent reaction ^{2}H(^{3}He, t), which was discussed in Sec. II B, the $d \rightarrow {}^2$He transition is in agreement with the IA-FSI model. The Watson-Migdal FSI underestimates the pp response at lower internal energies ($0.1\,{\rm MeV} \lesssim \varepsilon_{pp} \lesssim 0.2\,{\rm MeV}$) and overestimates the strength for $\varepsilon_{pp} \gtrsim 0.4$ MeV. Therefore, the di-proton acceptance corrections, which are applied to the ^{2}H(d,^{2}He)^2n spectra, assumed the IA-FSI model.

V. IMPULSE APPROXIMATION DESCRIPTION OF ^{2}H(d,^{2}He)^2n AND THE NEUTRON-NEUTRON SCATTERING LENGTH

From a formal point of view, reaction (4) belongs to the category of hadron-induced d-breakup processes and is therefore related to reaction (2). On the other hand it resembles reaction (3), because the (d,^{2}He) reaction mimics electron-capture as discussed in Refs. [2,4]. Note that the momentum transfer in muon-capture processes is higher ($q \approx 0.5$ fm^{-1}) than for electron capture, but the reaction mechanism is otherwise similar. A common feature of reactions (4), (3), and (1) is that they can be described in the impulse approximation [56,57].

A discussion regarding the measurement of a_{nn} with the "fundamental" reaction ^{2}H(n, p)^2n can be found in Ref. [22]. Relevant aspects of reaction (4) are

(i) The final state consists of four hadrons, which seems to make the reaction more difficult than the reactions discussed above. However, it was shown in Sec. II that ^{2}He can be treated as quasi-bound particle especially for the low ε region. That leaves three strongly interacting

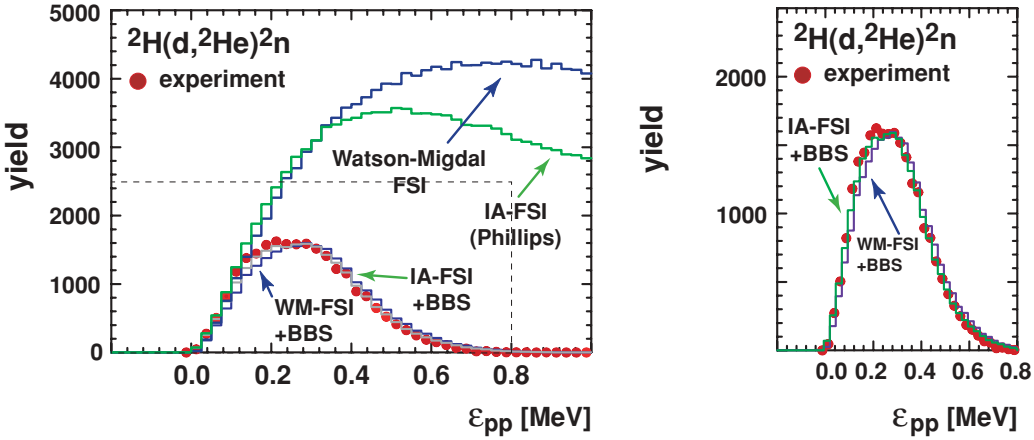

FIG. 6. (Color online) Measured and calculated distribution of the *pp* events as function of the internal energy ε_{pp}. Relative *nn* energies $\varepsilon_{nn} < 2$ MeV were considered for the experimental data. Filled circles represent experimental data points. No acceptance correction was applied. Left: Calculations of *pp* FSI according to the Watson-Migdal model and IA-FSI model by Phillips are indicated by solid curves. The predictions of these models folded with the limited acceptance of the BBS are shown, too. Right: The area marked by a dashed rectangle in the left figure, is plotted again. The FSI models, which are acceptance corrected and which account for the experimental resolution of ε_{pp}, are plotted as solid curves.

particles in the final state. The $(d,^2\mathrm{He})$ reaction is used as spectroscopic tool for the di-neutron system.

(ii) As only the internal energy of the di-neutron system ε_{nn} is known and relative angles, etc. remain unobserved, reaction (4) measures ^2n in incomplete kinematics.

(iii) Because the momentum transfer to the di-neutron system is small in a measurement at $\Theta \approx 0^\circ$ ($q \approx 0.1$ fm^{-1}), the probability for a transfer of angular momentum $\Delta L > 0$ is low ($q\,r \approx 10^{-1}$). As a result, the $^1S_0$ configuration is significantly enhanced over configurations of higher partial waves.

(iv) The kinematics of the reaction ($E_d \approx 170$ MeV) is chosen such that $\varepsilon_{nn}, \varepsilon_{pp} \ll E_d$. The adiabatic approximation should therefore be valid to good approximation, i.e., the time scale for interactions within ^{2}He and ^2n is long compared to the time scale of the scattering process. Hence, the internal excitation of ^{2}He and ^2n is assumed to be unaffected by the interaction between ejectile and residual di-nucleon system. A similar argument holds for effects of three-nucleon forces.

(v) The initial state consists of two identical bosons. Consequently, the transition amplitude $\mathcal{T}_{fi}$ has to be symmetrized in a strict formal treatment. It is not the aim of this work to provide such a description. Phenomenological arguments are used instead. The transition amplitude $\mathcal{T}_{fi}(\pi - \Theta, \Phi + \pi)$ for a central collision, i.e., the process at maximum momentum transfer, is small compared to the corresponding transition amplitude $\mathcal{T}_{fi}(\Theta, \Phi)$ for the GT-type process. The exchange term, which accounts for the interchange $d \leftrightarrow d$, can, therefore, be neglected to good approximation. Only even partial waves contribute now to the entrance channel due to the symmetry of the projectile-target system. This reduces the number of possible spin couplings in the reaction and thus leads to an enhanced selectivity of $(d,^2\mathrm{He})$ as probe for GT response.

The transition amplitude in leading order IA now has the form

$$\mathcal{T}_{fi}^{DW}(\vec{k}_f, \vec{k}_i) = \int d^3q\, D(\vec{k}_f, \vec{k}_i, \vec{q}\,)\, t_{\sigma\tau}^{C}(\vec{q}\,)\rho_p^{\sigma\tau}(\vec{q}\,)\rho_{fi}^{\sigma\tau}(\vec{q}\,), \tag{26}$$

where $\rho_p^{\sigma\tau}(\vec{q}\,)$ has been defined in Eq. (17) and $\rho_{fi}^{\sigma\tau}(\vec{q}\,)$ is the corresponding transition density with $|\Psi_{^2\mathrm{He}}\rangle$ substituted by $|\Psi_{nn}\rangle$. The radial part of this wave function was given in Eq. (21). As target and projectile consist of two loosely bound nucleons and the momentum transfer imparted to them is small, the distortion function D can be approximated by the plane-wave limit $\delta(\vec{q} - \vec{k}_i + \vec{k}_f)$ (see Sec. II A). Cross sections for ^{2}He are defined according to Eqs. (16) and (24). The triple differential cross section for the $^2\mathrm{He} + n + n$ residual system is then defined like its equivalent $B + p + p$, substituting ε by ε_{nn} in Eq. (16). Neglecting spin degrees of freedom, a simple scaling between cross section and response of the *nn* system is derived

$$\frac{d^2\sigma}{d\Omega(nn - {}^2\mathrm{He})\, d\varepsilon_{nn}} \propto \sqrt{\varepsilon_{nn}} \left| \int d^3r\, \Phi_{nn}^{*}(\vec{r}, a_{nn}) e^{i\vec{q}\cdot\vec{r}}\, \Phi_d(\vec{r}) \right|^2 . \tag{27}$$

In principle the D-wave contribution of the deuteron ($P_D \approx 5\%$) could be transformed by a GT$^+$ transition to a D-state configuration of the *nn* system. It is, however, argued that just like a P-wave contribution the D state of the *nn* system resides at higher relative energies and is negligible at $\varepsilon_{nn} \lesssim 2$ MeV. Further, a DWBA calculation with ACCBA shows that the inclusion of the deuteron D wave for $d \rightarrow {}^2\mathrm{He}$ enhances the cross section for $^2\mathrm{H}(d,^2\mathrm{He})^2n$ by about 0.1%. The strength of the analog D-wave contribution for $d \rightarrow {}^2n$ should be similar. The D-wave configuration of the exit channel of $^2\mathrm{H}(d,^2\mathrm{He})^2n$ is therefore expected to be small. Transitions mediated by the tensor force $t_{\sigma\tau}^{T}$, which have a $\Delta L \neq 0$ character, are also

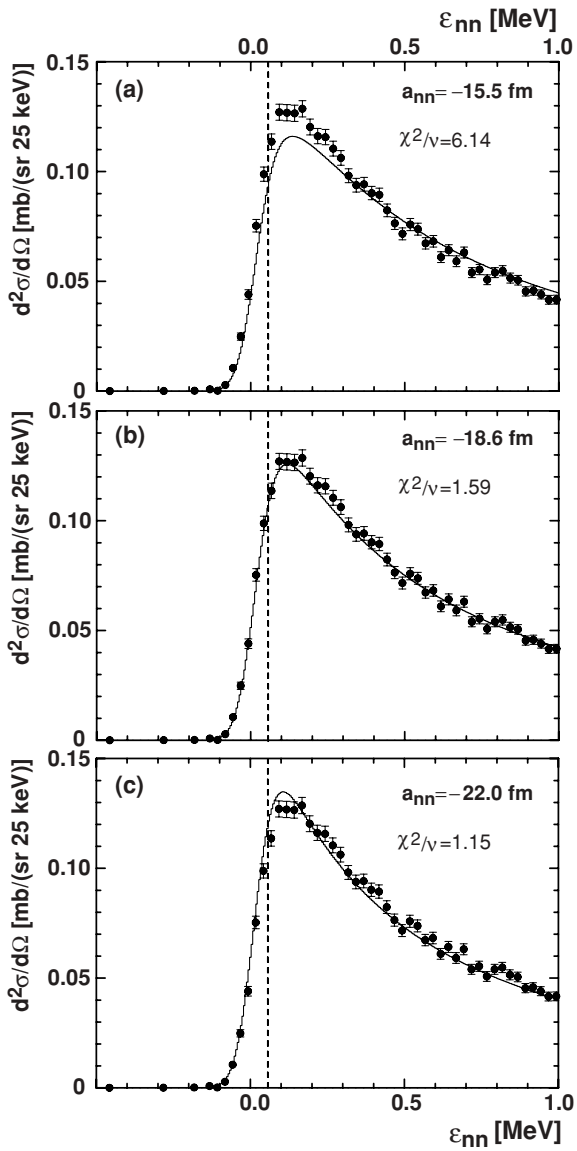

FIG. 7. Comparison of IA calculations with data from the ^{2}H(d,^{2}He)^2n reaction. The experimental data, which were extrapolated to $q = 0$, are represented by filled circles. The error bars indicate only statistical errors. The dashed vertical lines indicate the lower boundary of the data which were considered in the fits. Calculations have been performed in lowest order impulse approximation with $a_{nn} = -15.5$ fm (a), $a_{nn} = -18.6$ fm (b), and $a_{nn} = -22.0$ fm (c) and are indicated as solid curves.

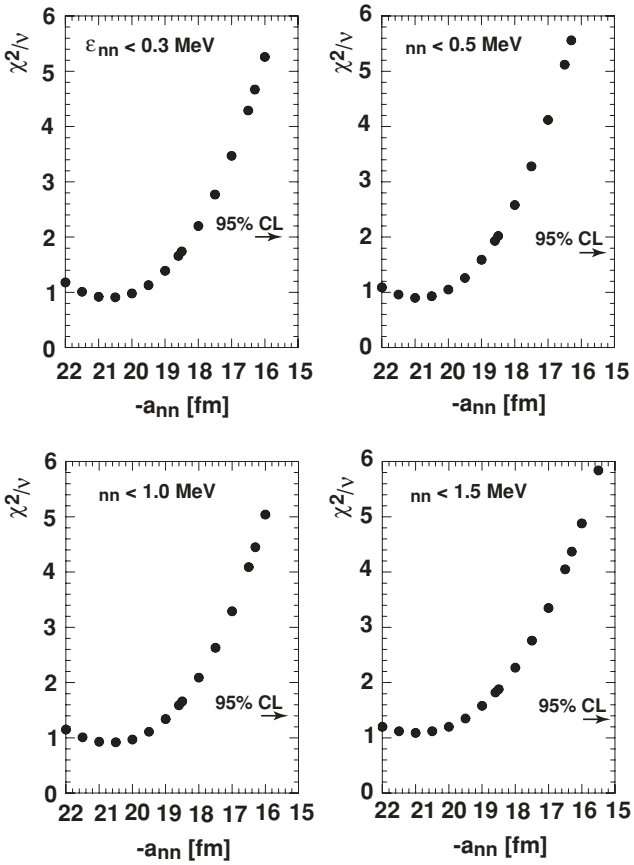

FIG. 8. Goodness of fit of IA calculations and experimental data ($q = 0$). The quantity χ^2/ν ($\nu =$ degrees of freedom) was computed taking into account the statistical errors of the data. The fitting procedure has been performed for $\varepsilon_{nn} < 0.3$ MeV (top left), $\varepsilon_{nn} < 0.5$ MeV (top right) $\varepsilon_{nn} < 1.0$ MeV (bottom left), and $\varepsilon_{nn} < 1.5$ MeV (bottom right). The arrows indicate a confidence level (CL) of 95% at the position of the corresponding χ^2/ν. Note that for the extraction of a_{nn} a systematic error was assumed which is not incorporated in this figure.

expected to be small compared to the corresponding transitions of the central part $t^C_{\sigma\tau}$ and will therefore also be neglected in the following discussion.

Equation (27) only describes a phase-space weighted GT$^+$ strength function for ^{2}H(d,^{2}He)^2n, and the scattering length a_{nn} is extracted through a fit of Eq. (27) to the measured cross section spectrum. The interval of ε_{nn} considered in the comparison is defined according to the following arguments. At internal energies $\varepsilon_{nn} \to 0$ the nn response is forced to 0 by the decreasing phase space ($\propto\sqrt{\varepsilon_{nn}}$) and is also determined by the experimental energy resolution. So the beginning of the rising edge (see Fig. 5) contains almost no information about a_{nn}. The most sensitive region for a_{nn} is the maximum of the nn response, as can be seen from Eq. (22). Thus, good resolution is of significant importance. We assumed the region of interest to start at an internal energy ε_{nn} where the corresponding cross section reaches 90% of the maximum cross section. The lower boundary for the comparison is therefore set to $\varepsilon_{nn} = 0.065$ MeV, thereby cutting off the nn distribution at low energies. When considering higher internal energies ($\varepsilon_{nn} \gtrsim 0.1$ MeV), the term $(1/2)\, r_{nn}\, k^2$ of the effective range expansion [Eq. (22)] eventually determines the falloff of the nn response. For energies $\varepsilon_{nn} \gtrsim 1.0$ MeV higher orders of k may start to play a role and the experimental spectrum may also contain small contributions from P and D waves. There is, of course, no sharp boundary that marks the end of the validity of Eqs. (27) and (22). Therefore, four different kinds of fits with upper boundaries at 0.3 MeV, 0.5 MeV, 1.0 MeV, and 1.5 MeV, respectively, are performed. The calculated distributions were projected into energy bins of 25 keV width in accordance with

the binning of experimental spectra. As already mentioned above, the absolute strength of the *nn* distribution is a free parameter in the fit. The fitting algorithm minimizes the reduced chi square χ^2/ν (ν = number of degrees of freedom) [58]. The experimental spectrum to be fitted is the $q \to 0$ extrapolated spectrum of Eq. (27). Figure 7 shows three fits for $\varepsilon_{nn} < 1$ MeV with $a_{nn} = -15.5$ fm, -18.6 fm, -22.0 fm as examples. The IA prediction with $a_{nn} = -15.5$ fm does not reproduce the measured distribution of the *nn* response. The calculated distributions with $a_{nn} = -18.6$ fm, -22.0 fm agree with the experimental outcome ($\chi^2/\nu \approx 1$).

Several χ^2/ν distributions are displayed in Fig. 8. Fits were done for a_{nn} between -15.5 and -22.0 fm in steps of 0.5 fm. Additional fits were performed for the recommended value of a_{nn} (-18.6 fm) and for the result of the Bonn experiment (-16.3 fm) (both indicated at the appropriate positions). Independent of the upper boundary ($\varepsilon_{nn} < 0.3$ MeV, 0.5 MeV, 1.0 MeV, 1.5 MeV) the fits yield $\chi^2/\nu \approx 1$ for $a_{nn} \approx -20$ fm. The quality of the fits significantly deteriorates for $-a_{nn} \lesssim 17$ fm. We note that the diagrams in Fig. 8 change only slightly when the experimental spectrum at $0^\circ < \Theta_{\mathrm{c.m.}} \leqslant 1^\circ$ is compared with IA calculations that incorporate a finite momentum transfer q in Eq. (27), indicating the small extent of the reaction model dependence. However, a lowering of the present low-energy cut on ε_{nn} causes an overall upward shift of the χ^2/ν distributions of Fig. 8, because the steep gradient of the low energy edge leads to a mismatch of calculation and data.

In order to give a value for a_{nn} and a corresponding uncertainty from the experimental data, a 2% systematic error for the relative cross section ($\varepsilon_{nn} < 1.5$ MeV) is estimated. This error also accounts for a possible contribution of non-$^1S_0$ configurations in this region. Following a conservative approach, the systematic error is included in the fit, which results in a shift of the distributions of Fig. 8 to smaller χ^2/ν. Fits are assumed to be acceptable, if the chi-square probability function $\mathrm{P}(\chi^2) \geqslant 5\%$. Applying this criterion to all upper boundaries considered above yields $a_{nn} < -18.3$ fm. We note that the present experiment gives a lower limit for a_{nn} in a range that has clearly been ruled out previously.

VI. CONCLUSIONS AND OUTLOOK

The result of the present work agrees with the recommended value for a_{nn} (-18.6 fm) [17]. In light of the above result a value of -16.3 fm, as measured by the Bonn group [20], seems improbable. The corresponding χ^2/ν is 4.5 for $a_{nn} = -16.3$ fm ($\varepsilon_{nn} < 1.0$ MeV).

The analysis of the $^2\mathrm{H}(d,^2\mathrm{He})^2n$ reaction in terms of a_{nn} employed a rather simple model. The extraction of a_{nn} should be further improved with more elaborated reaction models. Such a model is, e.g., the refinement of the IA description used in this work. An example of this kind of model is discussed in Ref. [13] for $^2\mathrm{H}(p, p')d^*$. Alternatively, rigorous three-nucleon or four-nucleon calculations could be employed to predict the shape of the ε_{nn} distribution. Reference [59] presents rigorous three-nucleon calculations of $n + d$ breakup reactions and confronts the calculated distributions with measured proton spectra at forward angles (11.0 MeV $< E_n <$ 62.8 MeV). A further discussion is published in Ref. [60], where also the effects of three-nucleon forces on the high-energy proton spectra of $^2\mathrm{H}(n,p)^2n$ experiments have been considered. We refer to Refs. [61,62] for an overview of modern three-nucleon and four-nucleon calculations incorporating also the magnetic moment interaction between nucleons.

It is stressed that the present work employed the impulse approximation in lowest order, which is a quite simple approach. Although it was argued that this theory gives an adequate description for similar reactions, e.g., $^6\mathrm{Li}(d,^2\mathrm{He})$, a rigorous calculation is indispensable for a precise extraction of a_{nn}. The focus of this work is to provide the data of the $^2\mathrm{H}(d,^2\mathrm{He})^2n$ reaction, to demonstrate the selectivity of the probe $(d,^2\mathrm{He})$, and to show that, in principle, the neutron-neutron scattering length can be obtained from the measured cross section data.[1]

Note that fully microscopic calculations of the $d + d$ entrance channel at intermediate energies are needed for the CSB experiment $d + d \to {}^4\mathrm{He} + \pi^0$ as well [62,63].

Uncertainties regarding the reaction mechanism could be reduced, if the $^2\mathrm{H}(t,{}^3\mathrm{He})^2n$ reaction at intermediate energies is measured. Similar to $^2\mathrm{H}(n,p)^2n$ and $^2\mathrm{H}(d,^2\mathrm{He})^2n$, the forward-angle ^{3}He spectra are dominated by the $^1S_0$ configuration. This experiment can be performed at the National Superconducting Cyclotron Laboratory at Michigan State University, where a resolution of about 160 keV for $(t,^3\mathrm{He})$ charge-exchange reactions has been demonstrated [64].

It has been pointed out that some of the difficulties in the theoretical analyses could be overcome, if analog reactions leading to the *nn*,*np*, and *pp* FSI are analyzed with the same model [65]. This implies for the $^2\mathrm{H}(d,^2\mathrm{He})^2n$ reaction that high-resolution data of (p, p')-type reactions and (p, n)-type reactions at intermediate energies be available. A viable option to improve the quality of the (p, n)-type data is a $^2\mathrm{H}(^3\mathrm{He}, t)^2p$ measurement at RCNP ($E_{^3\mathrm{He}} \approx 450$ MeV) or KVI ($E_{^3\mathrm{He}} \approx 185$ MeV).

Another subject that can be tackled by means of $(d,^2\mathrm{He})$ reaction experiments addresses a fundamental issue of quantum mechanics. The question, if present quantum mechanics is a complete theory, has been originally asked in the seminal paper of Einstein, Podolsky and Rosen [66]. In order to furnish experimental data involving entangled fermions, a feasibility experiment to study spin correlations in hadronic systems has been performed with the $(d,^2\mathrm{He})$ mode of the BBS+ESN setup [67]. Singlet-spin proton pairs were generated in $^1\mathrm{H}(d,^2\mathrm{He})$ and $^{12}\mathrm{C}(d,^2\mathrm{He})^{12}\mathrm{B}$ (g.s.) charge-exchange reactions. Measured left/right asymmetries of secondary proton scattering on a carbon analyzer, which was placed within the FPP [68], form the experimental correlation function. This function can be tested with the prediction of quantum theory and confronted with inequalities, e.g., Bell-type

[1]The experimental data are available from the corresponding author (D.F.) on request.

inequalities, which local-hidden-variables models must satisfy [67,69].

VII. SUMMARY

The reaction ^{2}H(d,^{2}He)^2n has been measured at forward angles and interpreted in terms of the impulse approximation. It was shown that the reaction can be decomposed into the mirror transitions $d \rightarrow {}^2$He and $d \rightarrow {}^2n$, which in turn can be described by the overlap of their respective wave functions and a trivial phase-space factor. The neutron-neutron scattering length a_{nn} is obtained by comparing the measured cross section as a function of ε_{nn} with corresponding model calculations. Employing a simple theory, it turned out that $a_{nn} \leqslant -18.3$ fm (95% CL), i.e., $a_{nn}^N \leqslant -18.6$ fm [19]. In the hypothetical case that the electromagnetic interaction could be switched off, the interaction between two neutrons in the $^1S_0$ state would, thus, be more attractive than the interaction between two protons. This finding can guide and constrain models of charge symmetry breaking and phenomenological descriptions of the nucleon-nucleon force. It is noted that the result of the present experiment is in line with most of the recent experiments which obtained a value for a_{nn} [15,16,18].

ACKNOWLEDGMENTS

We wish to thank Dr. S. Brandenburg and the KVI accelerator staff. This work was performed with support from the Land Nordrhein-Westfalen and the EU under Contract No. TMR-LSF HPRI-1999-CT-00109. It was further performed as part of the research program of the Stichting FOM with financial support from the Nederlandse Organisatie voor Wetenschappelijk Onderzoek and as part of the research program of the Fund for Scientific Research–Flandres. This work has further been supported by the Deutsche Forschungsgemeinschaft DFG under Contract No. SFB 634.d.

[1] D. P. Stahel, R. Jahn, G. J. Wozniak, and J. Cerny, Phys. Rev. C **20**, 1680 (1979).
[2] S. Rakers *et al*., Phys. Rev. C **65**, 044323 (2002).
[3] E. W. Grewe *et al*., Phys. Rev. C **69**, 064325 (2004).
[4] C. Bäumer *et al*., Phys. Rev. C **68**, 031303(R) (2003).
[5] H. Okamura *et al*., Phys. Lett. **B345**, 1 (1995).
[6] T. Sams, C. Ellegaard, C. Gaarde, J. S. Larsen, J. L. Boyard, T. Hennino, J. C. Jourdain, B. Ramstein, M. Roy-Stephan, P. Radvanyi *et al*., Phys. Rev. C **51**, 1945 (1995).
[7] C. Ellegaard *et al*., Phys. Rev. Lett. **59**, 974 (1987).
[8] S. Kox *et al*., Nucl. Phys. **A556**, 621 (1993).
[9] A. Stricker, Y. Saji, Y. Ishizaki, J. Kokame, H. Ogata, T. Suehiro, I. Nonaka, Y. Sugiyama, S. Shirato, and N. Koori, Nucl. Phys. **A190**, 284 (1972).
[10] V. Kulkarni, J. Rapaport, R. W. Finlay, G. Randers-Pehrson, and R. D. Koshel, Nucl. Phys. **A367**, 157 (1981).
[11] N. Koori, M. Hyakutake, M. Matoba, H. Ijiri, Y. Fujita, Y. Uozumi, S. Shirato, T. Motobayashi, T. Ohsawa, and K. Sagara, Nucl. Instrum. Meth. Phys. Res. A **287**, 737 (1989).
[12] N. Matsuoka, T. Nora, A. Okihana, M. Yosoi, H. Okamura, H. Sakai, F. Hiei, M. Iwaki, and H. Sakaguchi, RCNP Annual Report **1987**, p. 23 (1987).
[13] S. Burzynski, K. P. Jackson, W. P. Alford, J. E. Cromer, R. Helmer, B. E. King, I. Šlaus, B. Spicer, A. Trudel, and S. Yen, Nucl. Phys. **A570**, 722 (1994).
[14] B. Gabioud *et al*., Phys. Rev. Lett. **42**, 1508 (1979).
[15] O. Schori, B. Gabioud, C. Joseph, J. P. Perroud, D. Rüegger, M. T. Tran, P. Truöl, E. Winkelmann, and W. Dahme, Phys. Rev. C **35**, 2252 (1987).
[16] C. R. Howell *et al*., Phys. Lett. **B444**, 252 (1998).
[17] R. Machleidt and I. Šlaus, J. Phys. G **27**, 69 (2001).
[18] D. E. Gonzáles Trotter *et al*., Phys. Rev. Lett. **83**, 3788 (1999).
[19] G. A. Miller, B. M. K. Nefkens, and I. Šlaus, Phys. Rep. **194**, 1 (1990).
[20] V. Huhn, L. Wätzold, C. Weber, A. Siepe, W. von Witsch, H. Witała, and W. Glöckle, Phys. Rev. Lett. **85**, 1190 (2000).
[21] V. Huhn, L. Wätzold, C. Weber, A. Siepe, W. von Witsch, H. Witała, and W. Glöckle Phys. Rev. C **63**, 014003 (2000).
[22] I. Šlaus, Y. Akaishi, and H. Tanaka, Phys. Rep. **173**, 257 (1989).
[23] D. F. Measday, Phys. Rep. **354**, 243 (2001).
[24] W. G. Love and M. A. Franey, Phys. Rev. C **24**, 1073 (1981).
[25] M. A. Franey and W. G. Love, Phys. Rev. C **31**, 488 (1985).
[26] F. Osterfeld, Rev. Mod. Phys. **64**, 491 (1992).
[27] G. F. Bertsch and H. Esbensen, Rep. Prog. Phys. **50**, 607 (1987).
[28] H. Okamura, Phys. Rev. C **60**, 064602 (1999).
[29] R. J. de Meijer and R. Kamermans, Rev. Mod. Phys. **57**, 147 (1985).
[30] J. N. Bahcall and R. M. May, Astrophys. J. **155**, 501 (1969).
[31] M. Kamionkowski and J. N. Bahcall, Astrophys. J. **420**, 884 (1994).
[32] R. J. N. Phillips, Nucl. Phys. **A53**, 650 (1964).
[33] M. J. Moravcsik, Nucl. Phys. **A7**, 113 (1958).
[34] R. B. Wiringa, V. G. J. Stoks, and R. Schiavilla, Phys. Rev. C **51**, 38 (1995).
[35] E. E. Gross, E. V. Hungerford, J. J. Malanify, and R. Woods, Phys. Rev. C **1**, 1365 (1970).
[36] K. M. Watson, Phys. Rev. **88**, 1163 (1952).
[37] A. B. Migdal, JETP **1**, 2 (1955).
[38] B. J. Morton, E. E. Gross, E. V. Hungerford, J. J. Malanify, and A. Zucker, Phys. Rev. **169**, 825 (1968).
[39] H. Sakai *et al*., Phys. Rev. C **35**, 344 (1987).
[40] H. Sakai *et al*., Nucl. Phys. **A631**, 757c (1998).
[41] P. Moskal, M. Wolke, A. Khoukaz, and W. Oelert, Prog. Part. Nucl. Phys. **49**, 1 (2002).
[42] E. Baumgartner, H. E. Conzett, E. Shield, and R. J. Slobodrian, Phys. Rev. Lett. **16**, 105 (1966).
[43] S. Rugmai, J. S. Al-Khalili, R. C. Johnson, and J. A. Tostevin, Phys. Rev. C **60**, 027002 (1999).
[44] D. V. Bugg and C. Wilkin, Phys. Lett. **B152**, 37 (1985).
[45] D. V. Bugg and C. Wilkin, Phys. Lett. **B154**, 243 (1985).
[46] D. V. Bugg and C. Wilkin, Nucl. Phys. **A467**, 575 (1987).
[47] P. Haefner, Master's thesis, Institut für Kernphysik Münster, 2004.

[48] P. Haefner *et al*., Evidence for a Soft Dipole Resonance in the Halo Nucleus ^{6}He (to be published).
[49] A. M. van den Berg, Nucl. Instrum. Meth. Phys. Res. B **99**, 637 (1995).
[50] H. J. Wörtche and EUROSUPERNOVA Collaboration, Nucl. Phys. **A687**, 321 (2001).
[51] V. M. Hannen *et al*., Nucl. Instrum. Meth. Phys. Res. A **500**, 68 (2003).
[52] S. Rakers *et al*., Nucl. Instrum. Meth. Phys. Res. A **481**, 253 (2002).
[53] R. Zegers and B. Kharraja, Raytracing at the Big-Bite Spectrometer, KVI internal report 206i, 1998.
[54] V. M. Hannen, Ph.D. thesis, Rijksuniversiteit Groningen, 2001.
[55] C. Bäumer *et al*., Phys. Rev. C **63**, 037601 (2001).
[56] K. W. McVoy, Phys. Rev. **121**, 1401 (1961).
[57] M. Bander, Phys. Rev. **134**, 1052 (1964).
[58] J. L. Chuma, computer program PHYSICA, reference manual and user's guide, TRIUMF, 1998.
[59] W. Tornow, R. T. Braun, and H. Witała, Phys. Lett. **B318**, 281 (1993).
[60] H. Witała, J. Golak, W. Tornow, W. Glöckle, and D. Hüber, Phys. Rev. C **51**, 1095 (1995).
[61] A. Kievsky, M. Viviani, L. E. Marcucci, and S. Rosati, Nucl. Phys. **A737**, 61 (2004).
[62] M. Viviani, A. Kievsky, and S. Rosati, Nucl. Phys. **A737**, 205 (2004).
[63] E. J. Stephenson *et al*., Phys. Rev. Lett. **91**, 142302 (2003).
[64] B. M. Sherrill *et al*., Nucl. Instrum. Meth. Phys. Res. A **432**, 299 (1999).
[65] W. T. van Oers and I. Šlaus, Phys. Rev. **160**, 853 (1967).
[66] A. Einstein, B. Podolsky, and N. Rosen, Phys. Rev. **47**, 777 (1935).
[67] S. Hamieh *et al*., J. Phys. G **30**, 481 (2004).
[68] V. M. Hannen *et al*., Nucl. Instrum. Meth. Phys. Res. A **500**, 68 (2003).
[69] C. Polachic *et al*., Phys. Lett. **A323**, 176 (2004).